

Rohitukine inhibits in vitro adipogenesis arresting mitotic clonal expansion and improves dyslipidemia in vivo[§]

Salil Varshney,* Kripa Shankar,* Muheeb Beg,* Vishal M. Balaramnavar,[†] Sunil Kumar Mishra,[†] Pankaj Jagdale,[§] Shishir Srivastava,[†] Yashpal S. Chhonker,** Vijai Lakshmi,^{††} Bhushan P. Chaudhari,[§] Rabi Shankar Bhatta,** Anil Kumar Saxena,[†] and Anil Nilkanth Gaikwad^{1,*}

Division of Pharmacology* and Medicinal and Process Chemistry Division,[†] Council of Scientific & Industrial Research-Central Drug Research Institute, Sector 10, Jankipuram Extension, Lucknow, Uttar Pradesh 226031, India; Regulatory Toxicology Group,[§] Council of Scientific & Industrial Research-Indian Institute of Toxicology Research, Lucknow, Uttar Pradesh 226001, India; Pharmacokinetics and Metabolism Division,** Council of Scientific & Industrial Research-Central Drug Research Institute, 10/1, Sector 10, Jankipuram Extension, Lucknow, Uttar Pradesh 226031, India; and Department of Biochemistry,^{††} King George's Medical University, Chowk Area, Lucknow, Uttar Pradesh 226003, India

Abstract We developed a common feature pharmacophore model using known antiadipogenic compounds (CFPMA). We identified rohitukine, a reported chromone anticancer alkaloid as a potential hit through in silico mapping of the in-house natural product library on CFPMA. Studies were designed to assess the antiadipogenic potential of rohitukine. Rohitukine was isolated from *Dysoxylum binacteriferum* Hook. to ≥95% purity. As predicted by CFPMA, rohitukine was indeed found to be an antiadipogenic molecule. Rohitukine inhibited lipid accumulation and adipogenic differentiation in a concentration- and exposure-time-dependent manner in 3T3-L1 and C3H10T1/2 cells. Rohitukine downregulated expression of PPAR γ , CCAAT/enhancer binding protein α , adipocyte protein 2 (aP2), FAS, and glucose transporter 4. It also suppressed mRNA expression of LPL, sterol-regulatory element binding protein (SREBP) 1c, FAS, and aP2, the downstream targets of PPAR γ . Rohitukine arrests cells in S phase during mitotic clonal expansion. Rohitukine was bioavailable, and 25.7% of orally administered compound reached systemic circulation. We evaluated the effect of rohitukine on dyslipidemia induced by high-fat diet in the hamster model. Rohitukine increased hepatic expression of liver X receptor α and decreased expression of SREBP-2 and associated targets. Rohitukine decreased hepatic and gonadal lipid accumulation and ameliorated dyslipidemia significantly. **In summary, our strategy to identify a novel antiadipogenic molecule using CFPMA successfully resulted in identification of rohitukine, which confirmed antiadipogenic activity and also exhibited in vivo antidyslipidemic activity.—**

Varshney, S., K. Shankar, M. Beg, V. M. Balaramnavar, S. K. Mishra, P. Jagdale, S. Srivastava, Y. S. Chhonker, V. Lakshmi, B. P. Chaudhari, R. S. Bhatta, A. K. Saxena, and A. N. Gaikwad. **Rohitukine inhibits in vitro adipogenesis arresting mitotic clonal expansion and improves dyslipidemia in vivo.** *J. Lipid Res.* 2014. 55: 1019–1032.

Supplementary key words S-phase arrest • *Dysoxylum binacteriferum* Hook. f. • 3T3-L1 • C3H10T1/2

Obesity and associated disorders have shifted from an epidemic state to pandemic proportions (1). Although factors responsible for obesity are still unclear, the increase in lipid content of adipocytes is considered relevant. These cells constitute roughly 1/6 of body weight and are involved in both catabolic and anabolic processes. By virtue of their capacity to secrete various adipokines and cytokines, adipocytes have gained the status of an important endocrine tissue (2). In a constant renewal process, ~50% of subcutaneous adipocytes are replaced every 8 years (3); thus, adipocytes are a good target for pharmacological intervention of obesity. Many natural products like genistein,

Abbreviations: aP2, adipocyte protein 2; C/EBP, CCAAT/enhancer binding protein; CFPMA, common feature pharmacophore model using known antiadipogenic compounds; GLUT, glucose transporter; HBAL, hydrogen bond acceptor lipid; HBD, hydrogen bond donor; HDL-c, HDL cholesterol; HFD, high-fat diet; HMGCoA R, HMG-CoA reductase; Hypo., hypothesis; LA, least active; LDL-c, LDL cholesterol; LDL R, LDL receptor; LXR, liver X receptor; MA, most active; MCE, mitotic clonal expansion; MDI, cDMEM media containing 3-isobutyl-1-methylxanthine, dexamethasone, and insulin; ORO, Oil Red O; PFD, pair-fed diet; RA, ring aromatic; SAB, sodium acetate buffer; SREBP, sterol-regulatory element binding protein; TC, total cholesterol.

¹To whom correspondence should be addressed.

e-mail: anil_gaikwad@cdri.res.in

[§]The online version of this article (available at <http://www.jlr.org>) contains supplementary data in the form of data, four figures, and one table.

This work was supported by Council of Scientific & Industrial Research-Central Drug Research Institute (CSIR-CDRI) Network project "Towards holistic understanding of complex diseases: Unraveling threads of complex disease (Thunder Project No. BSC0102" and partly by Department of Biotechnology (DBT) Project GAP0079. Financial fellowship/support was provided by Thunder (S.V.), DBT-SRF (M.B.), UGC-JRF (K.S.), ICMR-SRF (V.M.B. and Y.S.C.), and CSIR-SRF (S.K.M. and S.S.). Support from the flow cytometry facility of SAIF CSIR-CDRI is acknowledged. The authors declare no conflicts of interest. This manuscript bears CDRI communication number 8679.

Manuscript received 30 May 2013 and in revised form 28 February 2014.

Published, JLR Papers in Press, March 19, 2014

DOI 10.1194/jlr.M039925

conjugated linolenic acid, docosahexanoic acid, epigallocatechin gallate (EGCG), quercetin, resveratrol, and ajoene affect adipogenic differentiation at various life cycle stages of adipocytes (4–10). These effects are exerted either by induction of apoptosis, inhibition of adipogenesis, stimulating lipolysis, or combinations thereof (11). Although many compounds are reported to have antiadipogenic activity, systematic analysis of the structure and activity relationship based on common features is still a knowledge gap. This can be performed by different molecular modeling tools such as SYBYL/comparative molecular field analysis (CoMFA) and comparative molecular similarity indices analysis (CoMSIA) and Catalyst (HypoGen Module for quantitative analysis and Hiphop Module for qualitative pharmacophore analysis) (12–14). Pharmacophore-based virtual screening methods have added advantage over CoMFA, CoMSIA, or docking in terms of screening speed and their tendency to retrieve more structurally diverse leads. Therefore, exploiting the literature on diverse antiadipogenic compounds, we developed and validated a Hiphop model to find common pharmacophore properties of antiadipogenic molecules [common feature pharmacophore model using known antiadipogenic compounds (CFPMA)]. We used this model to perform virtual screening of an in-house natural compound library in compliance with *a*) feature requirements of pharmacophore *b*) not reported earlier for antiadipogenic effects. We identified rohitukine as a potential hit candidate. Rohitukine is a chromone alkaloid reported to be isolated from *Dysoxylum binectariferum* Hook. f. (Maliaceae) and *Amoora rohituka*. It had earlier been reported for various biological activities, namely anti-inflammatory, anticancer, immunomodulatory, and antiulcer properties (15–20). Two of its analogs, Flavopiridol and P-276-00, are currently being evaluated in advanced phase 2 clinical trials for potential anticancer therapy (15). Many natural compounds like EGCG, genistein, and kaempferol, which show antiadipogenic potential, have also been found to be anticancer agents (21–23). Recently, there have been reports that establish an association between obesity and cancer (24–26). The phosphoinositide 3-kinase/protein kinase B/mammalian target of rapamycin (PI3K/AKT/mTOR) pathway is the key signaling pathway that links both obesity and cancer. As antiadipogenic activity of rohitukine was not reported earlier, it was intriguing to assess its antiadipogenic potential.

In the present study, we investigated the effects of rohitukine on adipocyte differentiation in 3T3-L1 and C3H10T1/2 cells under the influence of hormonal inducers. We measured effects in terms of lipid accumulation and changes in gene and protein level expression for various adipogenesis-associated markers. Moreover, we studied the effect of rohitukine in a high-fat diet (HFD)-fed Syrian golden hamster (*Mesocricetus auratus*) model of dyslipidemia. Our studies conclude that rohitukine affects the early phase of adipogenic differentiation by inhibiting AKT-mTOR phosphorylation and also leads to S-phase cell cycle arrest during mitotic clonal expansion (MCE). Rohitukine, at later time points, downregulates expression of

PPAR γ , CCAAT/enhancer binding protein (C/EBP) α , adipocyte protein 2 (aP2), FAS, and glucose transporter (GLUT) 4 and leads to inhibition of adipogenesis. Rohitukine also exhibited in vivo antidyslipidemic effects in the HFD-fed hamster model.

MATERIALS AND METHODS

Common feature pharmacophore model

Sixteen diverse compounds of varying antiadipogenic capacity were used as a training set (27). Pharmacophore was generated using the Hiphop algorithm of Catalyst implemented in the Discovery Studio 2.0 software (DS 2.0). All compounds used in the study were built using ISIS Draw 2.5 and imported to DS 2.0 Windows. These compounds were optimized using the CHARMM force field (14, 28, 29). The module of DS generated 255 diverse conformations of molecules with the energy cutoff range of 20 kcal/mol above the global minimum. The most potent compound (rutin) in the training set inhibited 83%, and the least active (LA) compound (sinapinic acid) 2.3% of total increased lipid accumulation during adipogenesis (27). The most active compound, rutin, was assigned a principal value of 2 and MaxOmitFeat value of 0 to insure that all features of this molecule are considered for generation of the hypothesis. For other molecules of the training set, principal and MaxOmitFeat values were set as 1 and 0. The minimum interfeature distance was set to 2 Å from the default value of 2.97 Å in order to consider the functional groups that are present in the training set compounds as closely as 2 Å. This was done to include the closely related functional groups present in the training set compounds (C = O and –OH) in carboxylic acid, which are present in most of the training set compounds involved in the 3T3-L1 inhibition. Feature mapping protocol was used to identify the common features present in the training set compounds. As predicted, hydrogen bond acceptor lipid [HBAL; minimum (min.) 1 to maximum (max.) 5], ring aromatic (RA; min. 1 to max. 5), and hydrogen bond donor (HBD; min. 1 to max. 5) were selected during the pharmacophore generation.

Extraction, fractionation, and isolation of pure compounds

Rohitukine was isolated and characterized as mentioned previously (16). Briefly, air-dried, powdered stem bark of *Dysoxylum binectariferum* (2.0 kg) was extracted with distilled ethanol (5 \times 5.0 liters) by cold percolation. The combined extracts were filtered and concentrated under reduced pressure below 50°C to a brown viscous mass. It was dried under high vacuum to remove the last traces of solvent yielding 80 g crude extract. Twenty grams of ethanolic extract was macerated and fractionated into *n*-hexane soluble (0.8 g), chloroform soluble (10.2 g), *n*-butanol soluble (4.2 g), and *n*-butanol insoluble (4.8 g) fractions. The MA chloroform soluble fraction on repeated chromatography yielded a known alkaloid, rohitukine (5,7-dihydroxy-2-methyl-8-[4-(3-hydroxy-1-methyl)piperidinyl]-4H-1-benzopyran-4-one). The compound was then characterized using infrared spectroscopy, nuclear magnetic resonance spectroscopy, mass spectrometry, derivatization, and comparison with the available literature. Purity was determined by HPLC and found to be >95%.

Differentiation of 3T3-L1 and C3H10T1/2 adipocytes

The 3T3-L1 and C3H10T1/2 cell lines were purchased from the American Type Culture Collection. Cells were cultured in a humidified atmosphere at 37°C and 5% CO₂ in DMEM containing

10% (v/v) heat-inactivated fetal bovine serum and penicillin-streptomycin antibiotics (cDMEM). For adipogenic induction, cells were seeded in 24-multiwell plates. Two days postconfluence, culture medium was replaced with differentiation medium [medium containing insulin 5 µg/ml, 3-isobutyl-1-methylxanthine 0.5 mM, and dexamethasone 250 nM (MDI)]. This medium was replaced after 48 h with medium containing 5 µg/ml insulin. This medium was replaced after 48 h, and cells were maintained in cDMEM. Lipid droplets started appearing from day 4, and >90% of cells showed lipid globules 6–8 days after induction. To study the effect of rohitukine on adipogenic differentiation, cells were differentiated at given concentrations and/or time exposed to rohitukine as indicated in the figures.

Oil Red O staining

Differentiated 3T3-L1 (with or without rohitukine) adipocytes were rinsed in PBS (pH 7.4). The adipocyte lipid globules were stained with Oil Red O (ORO; 0.36% in 60% isopropanol) for 20 min. Accumulated dye was extracted using 100% isopropanol, and absorbance was measured at 492 nm.

Western blotting

Cells were lysed in mammalian lysis buffer containing protease and phosphatase inhibitors (Roche). Similarly, tissues were freeze thawed and triturated in liquid nitrogen, and protein lysates were prepared using lysis buffer as mentioned previously. Protein lysates were denatured, and an equal quantity of protein was resolved by SDS-PAGE. It was electrotransferred to nitrocellulose paper. The membranes were blocked with 5% skimmed milk in Tris-buffered saline containing 0.05% Tween-20 (TBS-T). After washing with TBS-T, the membranes were incubated with target-protein-specific antibodies for 14 h at 4°C, followed by incubation with HRP-conjugated secondary antibodies for 1 h. The target proteins were detected using chemiluminescent substrate (Millipore) using Chemidoc (GE). For equal loading and normalization purposes, β-actin was used as internal control.

Real-time PCR

Total RNA was isolated from 3T3-L1 cells and tissues using TRIzol reagent (Invitrogen, CA). First strand cDNA synthesis was performed using Megascript reverse transcriptase kit (Applied Biosystems) and subsequently used for quantitative real-time PCR analysis on Light Cycler 480 (Roche Diagnostics). Statistical analysis of the quantitative real-time PCR was obtained using the ($2^{-\Delta\Delta Ct}$) method, which calculates the relative changes in gene expression of the target, normalized to an endogenous reference (GAPDH in vitro and β-actin for in vivo experiments) and relative to a calibrator that serves as a control group. Gene-specific primer pairs used in these studies are listed in **Table 1**.

Cell cycle analysis using flow cytometry

Two-day postconfluent 3T3-L1 preadipocytes were incubated in adipogenesis MDI with or without rohitukine at different concentrations. The cells were harvested after 24 h, washed, and resuspended in PBS. Then, cells were fixed in 70% ice-cold ethanol. Pelleted cells were suspended in propidium iodide for 30 min at room temperature. At least 10,000 events were acquired per sample on a flow cytometer (FACSCalibur, BD). Analysis was performed using Modfit software to determine the relative number of cells in G1, S, and G2/M phases.

Cell proliferation assay/[³H]thymidine uptake assay

To assess cell proliferation, [³H]thymidine incorporation was measured after induction of differentiation of 3T3-L1 with or

TABLE 1. Primer sequences used for real-time PCR gene expression studies

Gene Name	Primer Pairs
Mouse-specific primer pairs	
LPL	F 5'ttgtgaaatgccatgacaag3' R 5'cagatgctttctctctgtttgt3'
aP2	F 5'gaaaacgagatggtgacaacg3' R 5'gcccttcataaactctgtgg3'
SREBP-1c	F 5'tctccagactgtaggcaaatct3' R 5'agcctcagttaccactcct3'
FAS	F 5'caacatgggacaccctgag3' R 5'gttggaagtgcaggttag3'
PPAR γ	F 5'aagacaacggacaatacaca3' R 5'gggggtgatattggaactg3'
C/EBP α	F 5'aaacaacgcaactggaaga3' R 5'gaggcattgdcactggtc3'
Wnt3a	F 5'gagacatgggacacagtc3' R 5'gggaatcagatgggtcctg3'
GATA2	F 5'caccctatccctgtaac3' R 5'cagcagtagagagtaagagacacca3'
Hamster-specific primer pairs	
LXR α	F 5'tcagcatctctctgagaccgg3' R 5'tcattagcatccgtgggaaca3'
LDL R	F 5'gcagtggttctgtggctgacac3' R 5'gccatgcacaggtcca3'
HMGCR	F 5'gagctacattgtgcttggcg3' R 5'tcattagccaggctcac3'
SREBP-2	F 5'gcaagtggttctgcatgaa3' R 5'tggtgttctgactggtacgcc3'
LPL	F 5'gattcactttctgggactga3' R 5'gccactgtgcccgtacagaga3'
PPAR α	F 5'ggccaatggcatcaaaa3' R 5'ccttggcgaattctgtgagc3'
β-Actin	F 5'tgctgctccctgatgcctctg3' R 5'aggagagcgtgacccctcat3'

GATA2, GATA binding protein 2; HMGCR, HMG-CoA reductase; LDL R, LDL receptor; LXR, liver X receptor; SREBP, sterol-regulatory element binding protein; Wnt3a, Wingless-type MMTV integration site family, member 3A.

without rohitukine (20 µM) in the presence of 1 mCi of [³H]thymidine for 48 h. After that, cells were washed with PBS, once with ice-cold 10% TCA, and twice more with PBS. Cells were lysed in 2 N NaOH, and samples were analyzed after 24 h by scintillation counter.

Animals and diets

HFD (Cat. No. D12451, 45% kcal) was procured from Research Diets Inc. to induce dyslipidemia in 8-week-old (100–120 g body weight) Syrian golden hamsters (*M. auratus*). All experimental procedures were carried out as per the guidelines of Committee for the Purpose of Control and Supervision on Experiments on Animals, India, and approved by the Institutional Animal Ethics Committee.

A group of five animals was kept in controlled conditions. The animals with identification marks were acclimatized for 7 days before experimentation. The control group of hamsters was fed with normal chow diet. All other groups like HFD, pair-fed diet (PFD), and rohitukine-treated were fed with 45% kcal HFD for 10 days (day 1 to day 10). All groups had free access to diet and water. Fresh HFD kept at 4°C was administered daily (40 g diet/cage) at the same fixed time. The leftover diet of the previous day was weighed for the net food intake before being discarded. Likewise, the body weight of the animals was recorded daily before feeding and drug administration. Rohitukine was suspended in the 0.1% gum acacia solution and gavaged orally once daily at a fixed time for 7 consecutive days (days 4–10) to the treated group, and vehicle was administered to the parallel control.

Blood collection, plasma analysis, and histological analysis

The blood withdrawn from the retro-orbital plexus of anesthetized animals was collected in citrate-phosphate-dextrose containing microcentrifuge tubes, and plasma was separated. Total cholesterol (TC), HDL cholesterol (HDL-c), LDL cholesterol (LDL-c), and TGs were estimated from blood plasma using Cobas Integra 400™ Clinical Bio-analyzer (Roche Diagnostics). The sections of epididymal adipose tissue, pancreas, and liver were fixed in 10% formalin, dehydrated, and embedded in paraffin. Adipose tissue and liver sections were stained with hematoxylin and eosin (HE) to examine the morphology.

Pharmacokinetics studies: bioavailability estimation

In vivo pharmacokinetics study was performed in male Syrian golden hamsters (n = 3, weight range 120.0 ± 10 g). Oral and intravenous pharmacokinetics of rohitukine were carried out at 50 mg/kg and 5 mg/kg, respectively, for bioavailability estimation. Animals were kept on fasting overnight prior to dosing. Blood samples were collected from the retro-orbital plexus into microcentrifuge tubes containing heparin (20 IU/ml) as anticoagulant at 0.25–48.0 h post-oral dosing and 0.08–24 h post-intravenous dosing. Plasma separation was performed by centrifuging the blood samples at 2,000 g for 5 min. Plasma samples (300 µl) were extracted by the solid phase extraction method using 1 cc, C-18 (DSC-18, Supelco) cartridge. Cartridges were conditioned with 2 ml methanol and followed by 2 ml 10 mM sodium acetate buffer pH 5.5 (SAB). Plasma samples (300 µL) were diluted to 1 ml with SAB and then loaded into the cartridges. Then cartridges were washed with 2.0 ml of SAB. Analytes were eluted with 2 ml of methanol. The eluents were collected in glass tubes and evaporated to dryness under nitrogen in a water bath set at 40°C. These dry residues were finally reconstituted in 100 µl methanol, and 50 µl supernatant was injected to HPLC analysis. Rohitukine resolution and better peak shape were achieved on a Phenomex C₁₈ column (4.6 × 250 mm, particle size 5 µm) protected with a Phenomenex C₁₈ guard column. Phenacetin was used as internal standard (IS). The system was analyzed in isocratic mode with a mobile phase consisting of methanol-10 mM SAB (pH 5.5) 38:62, at a low rate of 1.0 ml/min. The absorption wavelength was set to 257 nm and 240 nm for rohitukine and IS, respectively. The pharmacokinetic parameters of plasma concentration-time profile were determined using the standard noncompartmental analysis module of WinNonlin (version 1.5, Pharsight, Mountain View, CA).

Statistical analysis

For in vivo studies, data were expressed as mean ± SEM, and for in vitro studies, data were expressed as mean ± SD; the Student's *t*-test was used for comparisons of measured parameters. Probability values of *P* < 0.05 (*), 0.01 (**), and 0.0001 (***) were used as measures of statistical significance. Data were analyzed on GraphPad Prism (Version 3.00, GraphPad Software Inc., San Diego, CA).

RESULTS

Rohitukine maps on CFPMA

The developed common feature pharmacophore models consisted of 3 main features, namely HBAL, RA, and HBD. Among the resulting 10 pharmacophore models with ranking scores ranging from 85.23 to 80.90 (Table 2), the top 5 pharmacophore models were analyzed for the best fit values of the training set molecules. Four out of the first 5 pharmacophore models had same features and interfeature distances, except the first hypothesis (Hypo-1) with RA [1] and HBAL [2], which had different orientations of groups in 3D space. To select the appropriate model, the predictability of Hypo-1 was analyzed against the remaining four hypotheses, which revealed that the third hypothesis (Hypo-3) predicted the most active, moderately active, and LA compounds better than the other four hypotheses (Fig. 1, fit value). Thus, on the basis of the predictability of the third hypothesis (Hypo-3) and the mapping of the MA and the LA compounds (Fig. 1), Hypo-3 was selected for further validation studies. The validation of this pharmacophore model was carried out using an external test set of 20 reported anti-adipogenic compounds that were not included in the training set. These compounds were screened on Hypo-3 using ligand pharmacophore mapping protocol using flexible fit method applying best conformation generation. The structures of these molecules were shown in the supplementary Fig. I. The Hypo-3 well predicts these external test set compounds in their respective classes. The fit value based prediction of these compounds are shown in (supplementary Table I). The selected hypothesis, Hypo-3 perfectly maps MA compound (rutin) with phenyl ring maps the

TABLE 2. Summary of hypothesis run

Hypo.	Features ^a	Rank	Direct Hit	Partial Hit	Max. Fit
1	RAA	85.024	1111111111111111	0000000000000000	3
2	RDA	84	1111111111111111	0000000000000000	3
3	RDA	83.013	1111111111111111	0000000000000000	3
4	RDA	82.187	1111111111111111	0000000000000000	3
5	RDA	82.185	1111111111111111	0000000000000000	3
6	RAA	82.18	1111111111111111	0000000000000000	3
7	RDA	81.838	1111111111111111	0000000000000000	3
8	RAA	81.231	1111111111111111	0000000000000000	3
9	RDA	81.213	1111111111111111	0000000000000000	3
10	RDA	80.891	1111111111111111	0000000000000000	3

Direct Hit (DH) indicates whether (1) or not (0) a training set molecule mapped every feature of the hypothesis. Similarly, Partial Hit (PH) indicates whether (1) or not (0) a molecule mapped to all but one feature in the hypothesis.

^aA, Hydrogen bond acceptor lipid (HBAL); Hydrophobic (H); Ring Aromatic (RA or R).

RA function of the pharmacophore, the oxygen atom of 4H chroman maps one HBA, and the hydroxyl group at the 3-[beta-L-rhamnopyranosyl-(1 → 6)-beta-D-glucopyranosyloxy] maps one HBD function. Further, this model was used as a contrivance for in-house library-based virtual screening of compounds that resulted in identification of the top-ranked lead, rohitukine, which was selected for further studies in the targeted activity. Rohitukine mapped to the highest fit value (2.88318) on Hypo-3 (Fig. 1) as compared with the MA compound (rutin) fit value (2.99981) of the training set. Thus, rohitukine maps well to the pharmacophore model (Hypo-3) where its hydroxyl (-OH) group of 3-hydroxy-1-methylpiperidin function present at position 8 of the basic chroman ring corresponds to the one HBD, the aromatic ring of its basic chroman ring feature as RA feature, and its carbonyl (C = O) function at the C-4 position of the chroman ring (chroman-4-one) fulfills the requirement of one HBA function.

Rohitukine inhibits adipogenesis

Varying concentrations of rohitukine (0–20 μM) were added to the MDI during differentiation. Microscopic

observation showed that rohitukine decreased lipid droplet accumulation in differentiated 3T3-L1 and C3H10T1/2 derived adipocytes in a concentration-dependent manner (Fig. 2A). Absorbance of extracted ORO accumulated in lipid droplets confirms that rohitukine inhibits adipogenesis significantly at a 5 μM concentration, and >80% of MDI-induced increased lipid accumulation was inhibited at a 20 μM concentration (Fig. 2B, C). At this concentration, rohitukine was found to be nontoxic in 3T3-L1 cells using MTT [3-(4,5-dimethylthiazol-2-yl)-2,5-diphenyltetrazolium bromide] based cell viability assay (data not shown). Rohitukine (20 μM) was added during days 0–2, 0–4, 0–6, 2–4, 2–6, and 4–6 of adipogenesis. Every rohitukine exposure condition led to decreased lipid accumulation in adipocytes, with a maximum inhibition at 0–6 days. Minimum exposure of 0–2 days was enough to yield significant decrease ($P < 0.001$) in lipid accumulation and adipogenesis in 3T3-L1 adipocytes (Fig. 2D–F). Consistent with these results, we observed that at a 20 μM concentration, mRNA expression levels of adipogenesis-associated genes, including PPARγ, aP-2, SREBP-1c, FAS, and LPL, were significantly reduced ($P < 0.01$); whereas a nonsignificant but decreasing trend was observed

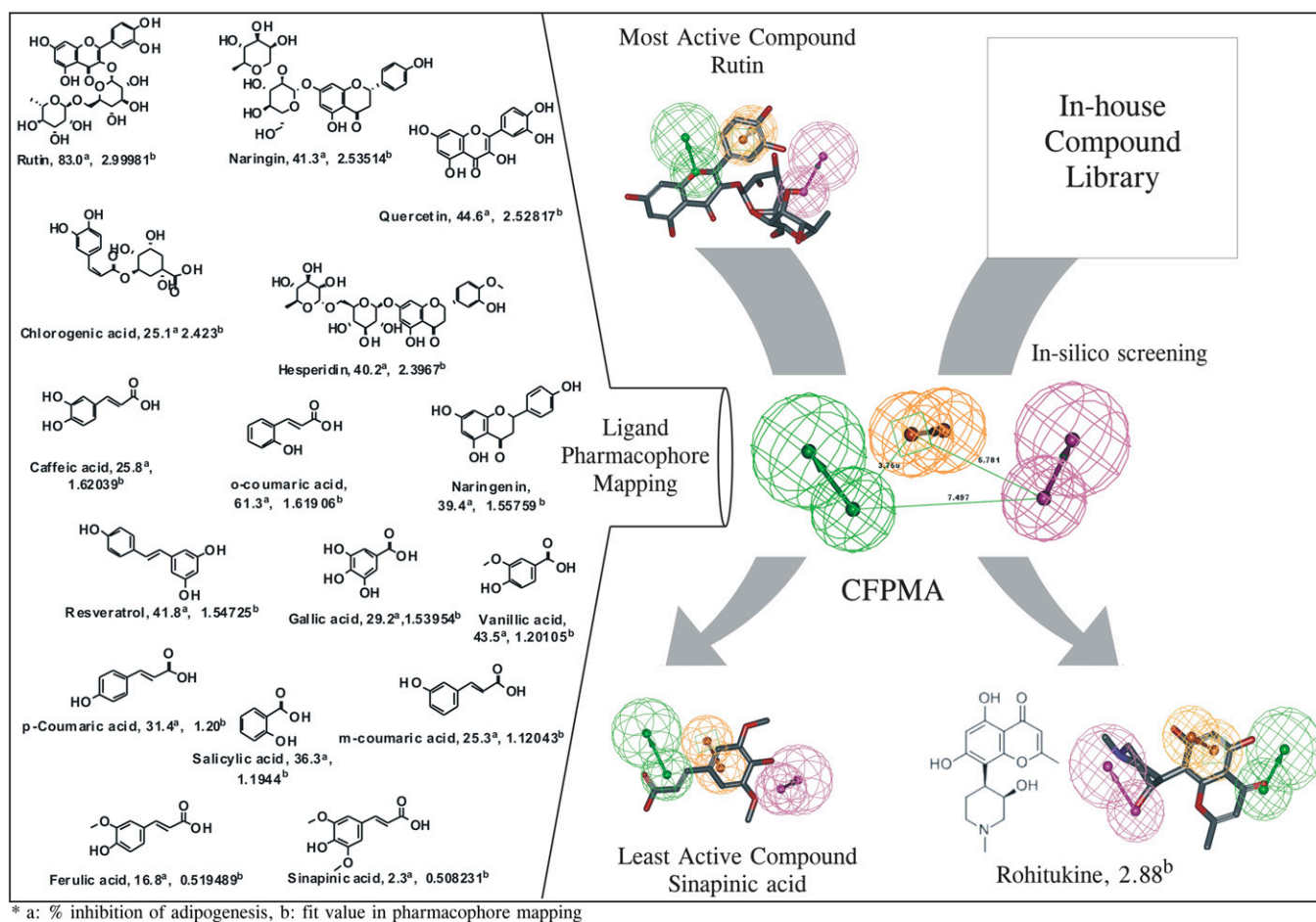


Fig. 1. The CFPMA pharmacophore model and in silico virtual screen. The common feature pharmacophore model was generated using a diverse set of antiadipogenic compounds. CFPMA is shown along with the inter-feature distance. The pharmacophore mapping of the MA compound, the LA compound (sinapinic acid), and virtual screen-identified hit rohitukine is shown. The actual % inhibition of MDI-induced lipid accumulation by molecule (a) that was used in model generation as well as fit value (b) generated on each molecule in pharmacophore mapping are shown next to the compound name.

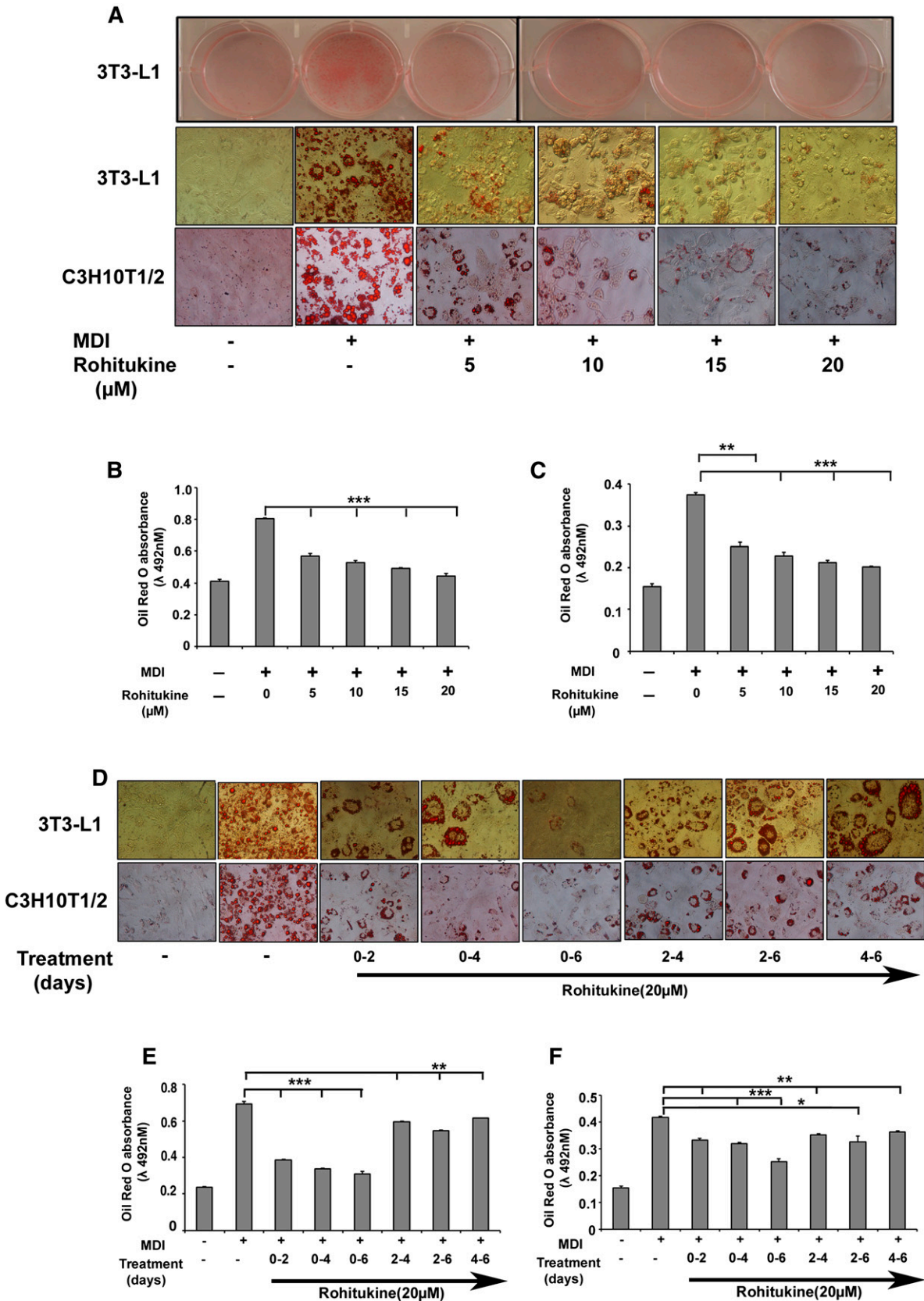


Fig. 2. Rohitukine inhibits adipogenesis. A: 3T3-L1 preadipocytes and C3H10T1/2 were cultured in the DMEM and MDI medium containing 0, 5, 10, 15, and 20 μ M rohitukine for 8 days. Culture dish images were acquired after lipid droplet staining with ORO; microscopic images were taken with Nikon Eclipse TI. Absorbance of extracted ORO accumulated in lipid droplets of 3T3-L1-derived (B) and C3H10T1/2-derived (C) adipocytes was measured spectrophotometrically at 492 nm. D: 3T3-L1 preadipocytes and C3H10T1/2 were cultured in the MDI medium with 20 μ M rohitukine for 0–2, 0–4, 0–6, 2–4, 2–6, and 4–6 days. The lipid droplets were stained with ORO, and

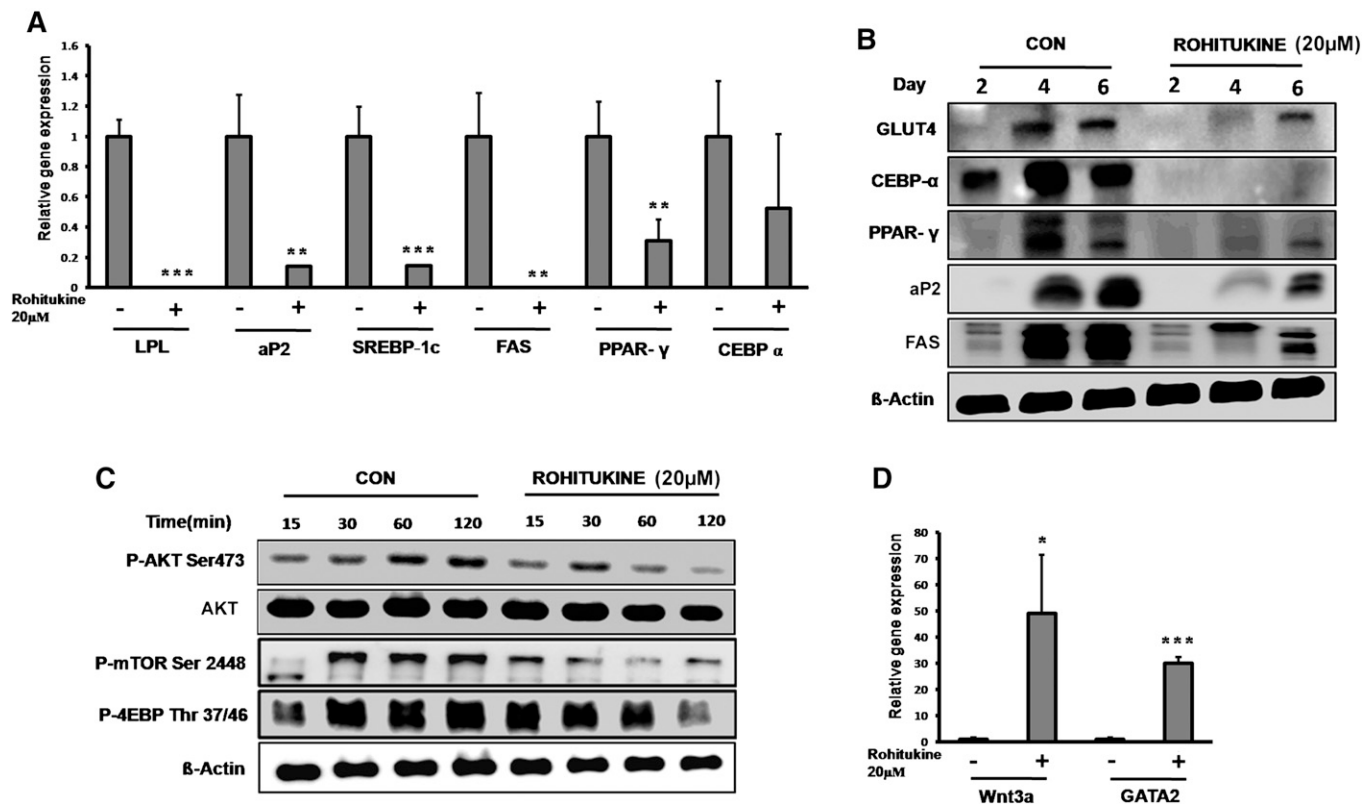


Fig. 3. Molecular markers of adipogenic inhibition. **A:** Relative mRNA abundance of LPL, aP2, SREBP-1c, FAS, PPAR γ , and C/EBP α on day 6 of adipocyte differentiation was measured by real-time PCR in the absence and presence of 20 μ M rohitukine in MDI. **B:** Rohitukine addition to MDI significantly downregulates the late phase protein level expression of GLUT-4, C/EBP α , PPAR γ , aP2, and FAS in 3T3-L1 adipocytes (i.e., on day 2, day 4, and day 6 of differentiation). **C:** Rohitukine inhibits early phosphorylation states of p-AKT (Ser473), mTOR (Ser2448), and 4EBP (Thr37/46) observed by Western blotting. **D:** Rohitukine increases the relative mRNA abundance of Wnt3a and GATA2 on day 2 measured by real-time PCR. The results were verified by three independent experiments, mean \pm SD. Significance of difference between the MDI-induced control and rohitukine-treated groups: * $P < 0.05$, ** $P < 0.01$, *** $P < 0.001$.

in the case of C/EBP α in real-time PCR analysis (Fig. 3A). This was also supported by the fact that protein level expression of PPAR γ , C/EBP α , aP2, FAS, and GLUT-4 expression was found to be suppressed significantly as compared with control during late phase (i.e., day 2, day 4, and day 6 of adipogenesis induction) (Fig. 3B). AKT phosphorylation, mTOR phosphorylation, and its target phosphorylation of 4EBP were reduced significantly in early rohitukine exposure (0–2 h) during adipogenesis (Fig. 3C). The gene expression of antiadipogenic transcription factors GATA2 and Wnt3a was increased significantly 30- and 50-fold by 48 h of rohitukine exposure (Fig. 3D).

Collectively, these results indicate that rohitukine possesses an antiadipogenic potential in vitro without any cytotoxic effect, and early 48 h exposure was sufficient for significant suppression of adipogenesis.

Rohitukine arrests MCE in S phase

When MDI was added to growth arrested confluent cells, it caused cells to enter into 2–3 rounds of the cell

cycle (i.e., MCE is prerequisite for adipogenesis). Addition of rohitukine to MDI perturbed MCE (Fig. 4A). At a 20 μ M concentration of rohitukine where maximum suppression of adipogenesis was observed, 41.15% of cells were in S phase compared with only 19.28% of cells treated with MDI alone (Fig. 4B). This highly significant increase demonstrates that cells either get delayed entry into S phase or get arrested in S phase.

MCE arrest was further evidenced in immunoblot expression analysis of cell cycle regulatory proteins performed at 16 and 24 h time points. Rohitukine causes reduction of cyclin-D, Cyclin Dependent Kinase (CDK)6, CDK4, cyclin-E, and CDK2 protein expression. These proteins are required to accomplish MCE in response to MDI induction. Furthermore, addition of rohitukine in MDI causes rescue of degradation of P27, as well as a reduced expression of C/EBP β , which can be attributed to inhibition of CDKs and MCE arrest, respectively (Fig. 4C). MCE blockade was also confirmed by [3 H]thymidine uptake assay. Rohitukine significantly inhibited MDI-induced [3 H]

microscopic images were taken with Nikon Eclipse TI. Absorbance of extracted ORO accumulated in lipid droplets of 3T3-L1-derived (E) and C3H10T1/2-derived (F) adipocytes was measured spectrophotometrically at 492 nm. All values are presented as the mean \pm SD of three experiments performed in triplicate. Statistical significance: * $P < 0.05$, ** $P < 0.01$, *** $P < 0.001$.

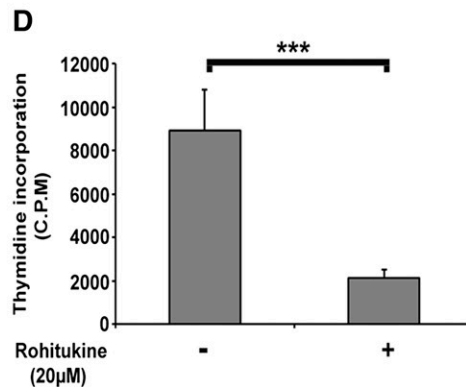
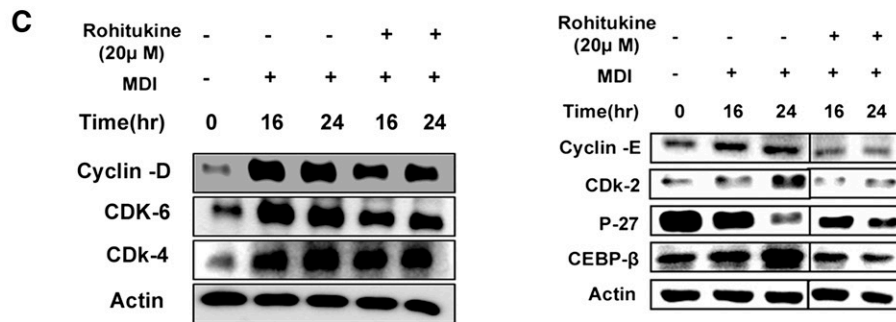
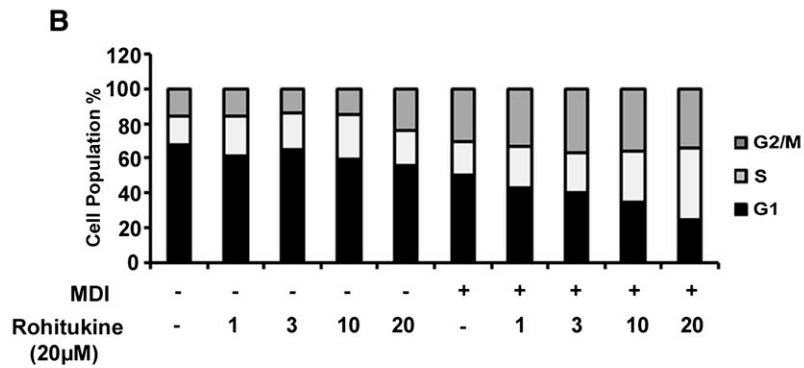
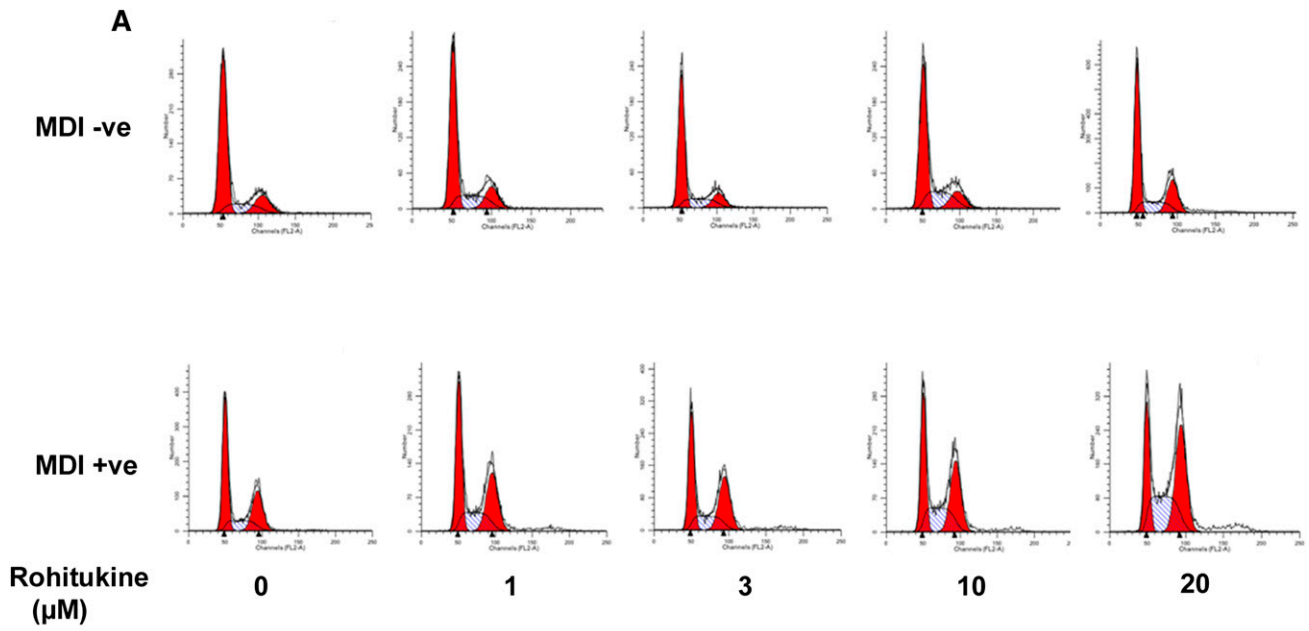


TABLE 3. Pharmacokinetic profile of rohitukine after oral (50 mg/kg) and intravenous (5 mg/kg) administration (n = 3)

Parameters	Estimates (mean ± SD)	
	Oral (50 mg/kg)	Intravenous (5 mg/kg)
C _{max} (µg/ml)	6.62 ± 0.66	5.37 ± 2.12
T _{max} (h)	0.25	—
AUC _{0-∞} (µg * h/ml)	10.66 ± 2.34	4.14 ± 1.08
MRT (h)	6.64 ± 1.39	7.07 ± 3.02
F _{abs} (%)	25.7	—

AUC, area under the curve from 0 to ∞ h; C_{max}, maximum concentration; F_{abs}, absolute bioavailability; MRT, mean residence time; T_{max}, time of maximum concentration.

thymidine incorporation after 48 h exposure (Fig. 4D) at a 20 µM concentration.

Oral bioavailability of rohitukine in hamster

The therapeutic response correlates with drug availability in systemic circulation. Bioavailability studies in rohitukine have not been reported yet. Oral bioavailability (50 mg/kg) was carried out in the Syrian golden hamster, which showed that rohitukine was readily bioavailable and that ~25.7% of rohitukine gets absorbed into systemic circulation when administered orally. It could be detected in plasma within 15 min post-oral dose and remained in circulation for more than 24 h (Table 3).

Rohitukine inhibits HFD-induced dyslipidemia in the Syrian golden hamster model

Initial experiments were designed to evaluate in vivo effects of rohitukine at 30 mg/kg and 100 mg/kg doses. We noticed the following major effects: *i*) very significant reduction of all lipid parameters like total TGs, TC, and LDL-c; and *ii*) reduced diet consumption as well as significant body weight loss (supplementary Fig. IV, A–H). These observations indicated that the lipid parameter reduction might be associated with decreased food intake due to anorexia, central regulation of appetite, or any other reason. To remove this variable, we planned a PFD group study to evaluate the true contribution of rohitukine toward associated lipid parameter changes. Compound dosing was initiated for 4 days in HFD-fed hamsters and continued until day 10. The PFD group was fed with an equivalent quantity of diet that was consumed by the rohitukine-treated group, but significant reduction in body weight gain was observed in the rohitukine-treatment group (Fig. 5A). Serum from the PFD group was collected a day later, and comparative lipid profiling was performed between PFD and rohitukine-treated groups. We observed significant reduction in TG, TC, and LDL-c levels (Fig. 5B–D). We also observed reduction in HDL levels in the rohitukine treatment group

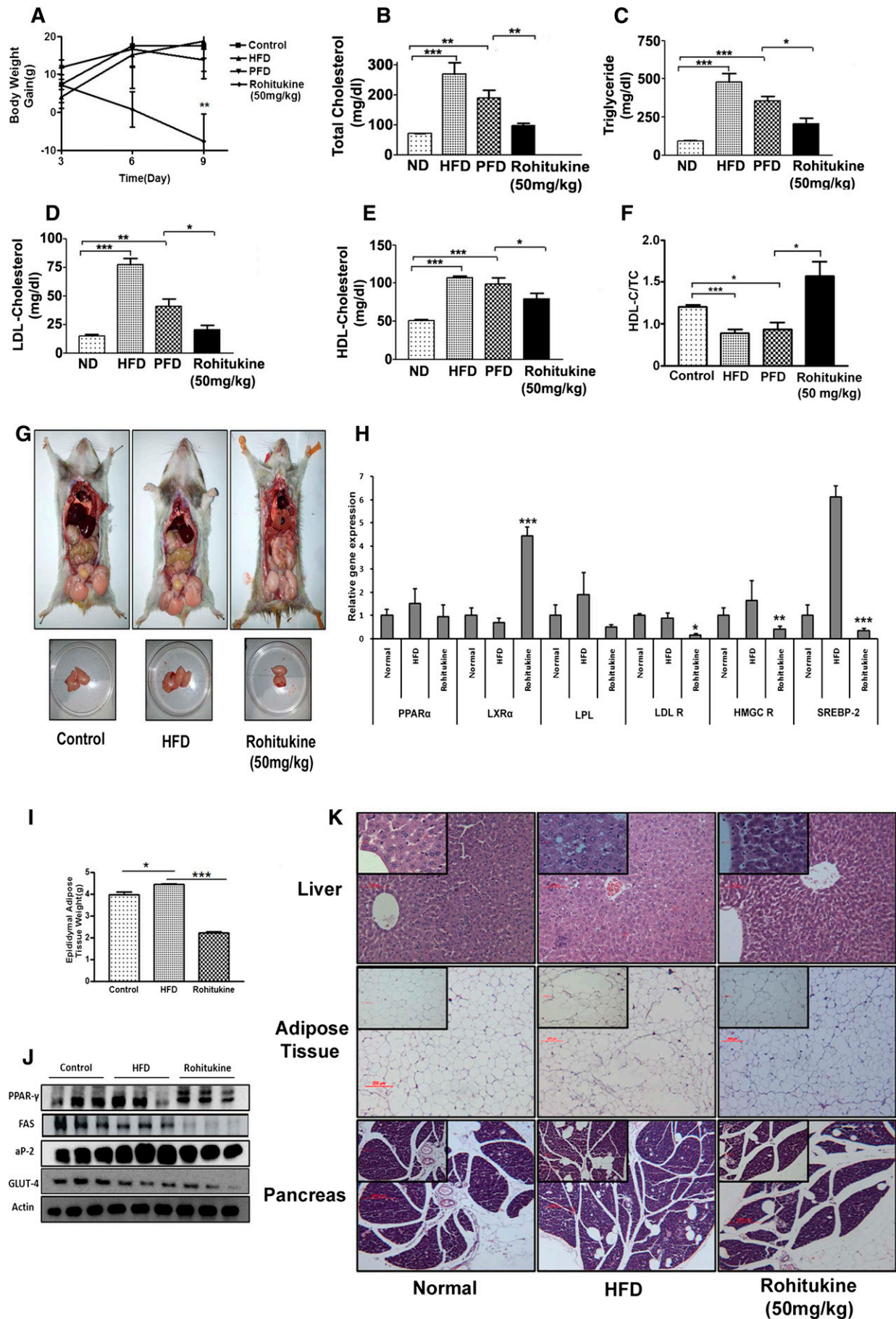
similar to earlier mentioned lipid parameters, but the HDL-c/TC ratio was significantly increased (Fig. 5E, F). We collected liver, pancreas, and adipose tissues of hamsters. Rohitukine increased hepatic LXRα mRNA expression ~4-fold, while expression levels of LDL R, HMGCR, and SREBP-2 were reduced significantly. However, we did not observe significant changes in the hepatic mRNA expression levels of PPARα and LPL (Fig. 5H). Epididymal fat tissue weight was significantly increased in the HFD-treated group, while it was reduced very significantly in the rohitukine-treated group (Fig. 5I). Protein level expression studies in adipose tissue showed PPARγ expression was reduced slightly, while significant reduction was observed in FAS, aP2, and GLUT-4 expression, exhibiting the effects of rohitukine on FA synthesis (Fig. 5J). Tissues were subjected to histological sectioning and staining. Careful observation showed that HFD-fed hamster adipocytes were hypertrophied compared with the rohitukine-treated group. We also observed more lipid droplet accumulation in the liver as usually seen in hepatic steatosis in HFD-fed animals. However, these droplets were absent in rohitukine-treated animals. In pancreatic tissue, we also observed more lipid/fat droplet accumulation in HFD-fed animals, which was reduced in the rohitukine-treated group (Fig. 5K).

DISCUSSION

In this study, we developed for the first time a CFPMA. We validated its predictability. Exploiting the potential of this model, we screened an in-house library of natural compounds and identified rohitukine as a top-ranking lead molecule. Indeed, rohitukine showed antiadipogenic activity in more than one cell model of in vitro adipogenesis. Rohitukine inhibition was prominent when added in the early phase of differentiation, possibly by affecting S-phase arrest in MCE. In vivo studies in rohitukine showed antidyslipidemic activity potentially affecting both liver and adipocyte metabolism.

Preadipocyte fibroblast clonal cell line 3T3-L1 is considered an excellent model system to identify molecules affecting adipogenesis. Many phytochemicals have been studied in great detail for their potential to inhibit adipogenesis and/or lipid accumulation capacities and have been reviewed comprehensively (11). Similarly, many phenolic and flavonoid compounds are able to inhibit lipogenesis and adipogenesis (27). In this study, we report a pharmacophore model built using a set of 16 chemically diverse compounds of natural and synthetic origin capable

Fig. 4. Effects of rohitukine on MDI-induced cell cycle progression in 3T3-L1 preadipocytes. A: Rohitukine arrested MDI-induced cell cycle progression in S phase. B: The population of cells in each stage of the cell cycle was quantified and showed concentration-dependent arrest in S phase. C: Postconfluent 3T3-L1 preadipocyte cells were incubated with MDI containing 20 µM rohitukine for 0, 16, and 24 h; rohitukine downregulated the expression of cyclin-D, CDK6, CDK4, cyclin-E, CDK2, C/EBPβ but stabilized P27 protein as observed by Western blotting. Represented cut blots were run, transferred, and exposed for the same time but separated away by unrelated samples. D: Rohitukine significantly inhibited the incorporation of [³H]thymidine into newly synthesized DNA after 48 h, measured by using a scintillation counter. The data are representative of three independent experiments that give similar results. Significance of differences between the MDI-induced control and rohitukine-treated groups: * *P* < 0.05, ** *P* < 0.01, *** *P* < 0.001.



of inhibiting adipogenesis (CFPMA). Our virtual screen efforts yielded 10 natural molecules out of which we screened the top-ranking hit at an initial concentration of 20 μ M. Rohitukine showed adipogenic inhibition in our primary assay. In subsequent investigations, rohitukine exhibited concentration-dependent as well as exposure-time-dependent decrease in ORO accumulation during 3T3-L1 and C3H10T1/2 adipogenic differentiation (Fig. 2).

In general, PPAR γ is considered a master regulator of adipogenic programming. C/EBP α and PPAR γ cross-regulate each other through positive feedback loops and transactivate downstream target genes such as aP2, LPL, and SREBP-1c (30, 31). GATA2 and GATA3 negatively regulate PPAR γ and C/EBP α expression and are thus responsible for decreased adipogenesis (32, 33). Similarly, the Wnt pathway is also a negative regulator of adipogenic induction (34). In general, rohitukine addition to differentiation media suppresses pro-adipogenic mRNA and protein expression and increases antiadipogenic gene expression (Fig. 3). It is noteworthy that *i*) maximum inhibition can be achieved at a concentration of 20 μ M, where total lipid accumulation was equivalent to undifferentiated cells, and *ii*) the activity at this concentration was limited but not exclusive to exposure to the compound in the early adipogenic phase. So, at this concentration of maximum suppression, we studied early signaling events during adipogenesis.

The PI3K-AKT pathway is involved in wide variety of metabolic actions (35). The AKT pathway gets upregulated in cancer (36). The rohitukine analog Flavopiridol inhibits the AKT signaling pathway and exerts its anticancer activity (37). AKT/mTOR activation is necessary for adipogenesis programming (38, 39). Adipogenic stimuli strongly induce AKT phosphorylation, which is sustained up to 2 h. Rohitukine (20 μ M) coincubation leads to significant suppression of AKT phosphorylation at the Ser473 residue. It was also found that mTOR phosphorylation at Ser2448 was reduced significantly. Rohitukine abrogates phosphorylation of the substrate of the AKT/mTOR pathway, 4EBP at Thr37/46, which is necessary for protein synthesis during adipogenesis. extracellular signal-regulated kinase (ERK) signaling has also been reported to be responsible for early adipogenic programming and has been the cause of inhibition of adipogenesis by C1q/tumor necrosis factor-related protein 11 (CTRP11), sulphoraphane-mediated adipogenic inhibition (40, 41). In our experiments, we could not see any rohitukine-mediated alteration in this pathway. Thus, rohitukine may exert

an antiadipogenic effect in very early phase signaling through the PI3K/AKT/mTOR pathway.

Phytochemicals such as piceatannol and resveratrol affected early insulin signaling events, which ultimately translated into inhibition of MCE (42–44). These changes in early signaling on hormonal induction are important in that they allow fully confluent cells to reenter clonal expansion. In view of early blocking in adipogenesis (Fig. 2D–F), we performed cell cycle regulation studies. As anticipated, we found a concentration-dependent cell number increase in S phase post 24 h of MDI induction (Fig. 4 A, B).

The cell cycle and its regulation play important roles in completion of MCE, which is a prerequisite for early adipogenesis. Activation and assembly of cyclin-D to CDK4 and 6, cyclin-E with CDK2, and degradation of the CDK inhibitor are required for G1/S-phase progression and to reenter MCE. Many natural compounds have been reported to inhibit adipogenesis by affecting MCE. Sulforaphane arrests cells in the G0/G1 phase (41); widdrol causes cell cycle arrest in the G1/S-phase transition (45); genistein, piceatannol, and curcumin arrest cells in the S/G2/M phase (46); and garcinol and pterostilbene cause G2/M-phase arrest (47). Rohitukine decreases CDK4, CDK6, CDK2, cyclin-D, and cyclin-E and stabilizes P27 levels (Fig. 4C), which can be corroborated to observed S-phase arrest in cell cycle analysis by flow cytometry. Furthermore, decreased C/EBP β expression further strengthens the phenomenon of adipogenesis inhibition in the early stage. Thus, to summarize, rohitukine modulated early phase adipogenesis and caused MCE arrest by modulation of cell cycle regulatory proteins (Fig. 6).

Once we established the antiadipogenic effects of rohitukine, we wanted to evaluate its effects in vivo. Incidentally, most of the compounds on which CFPMA was developed had also been reported for antidyslipidemic or hypolipidemic activity. Although these activities are distinct from each other, there is an observed link between them. The mechanisms of their interdependence are not very clear yet. Because adipose tissue and the liver are major organs contributing to overall lipid turnover in vivo, one can possibly corroborate the interdependence of antiadipogenic and antidyslipidemic activity. The MA antiadipogenic compound rutin was found to be antidyslipidemic when studied in the HFD hamster model (27, 48). Nar-ingen was proved to be hypolipidemic in the diet-induced hypercholesterolemia hamster model (49). Quercetin and resveratrol protect hypercholesterolemic hamsters against aortic fatty streak accumulation (50). The resveratrol analog

Fig. 5. Effect of rohitukine administration on normal chow diet (ND)-, HFD-, and PFD-fed dyslipidemic Syrian golden hamsters. A: Mean body weight gain of different groups showed that rohitukine significantly decreased body weight gain by the end of the experiment. Rohitukine showed significantly decreased TC (B), total TG (C), LDL-c (D), and HDL-c (E) compared with PFD. F: Rohitukine significantly increased the HDL-c/TC ratio. G: Rohitukine reduced gonadal fat mass as compared with the HFD-fed group. H: Hepatic mRNA expression levels in HFD-fed and HFD+rohitukine-fed (50 mg/kg) groups were analyzed at the end of the experiment. LXR α expression was increased significantly to 4-fold, while significant reduction was observed in LDL R, HMGCR, and SREBP-2 in the HFD+rohitukine-fed group. I: Significantly increased epididymal fat weight in the HFD-fed group is reduced significantly in the rohitukine-fed animal group. J: Protein level expression of PPAR γ , FAS, aP2, and GLUT4 in epididymal fat tissue in control, HFD-fed, and HFD+rohitukine-fed groups. K: HE staining of liver, adipose, and pancreas tissues. Images in the insets are magnified images from the same section. Rohitukine decreased the lipid accumulation in liver compared with HFD-fed animals. Each bar represents mean \pm SEM, with significance expressed as *** $P < 0.0001$, ** $P < 0.001$, * $P < 0.05$.

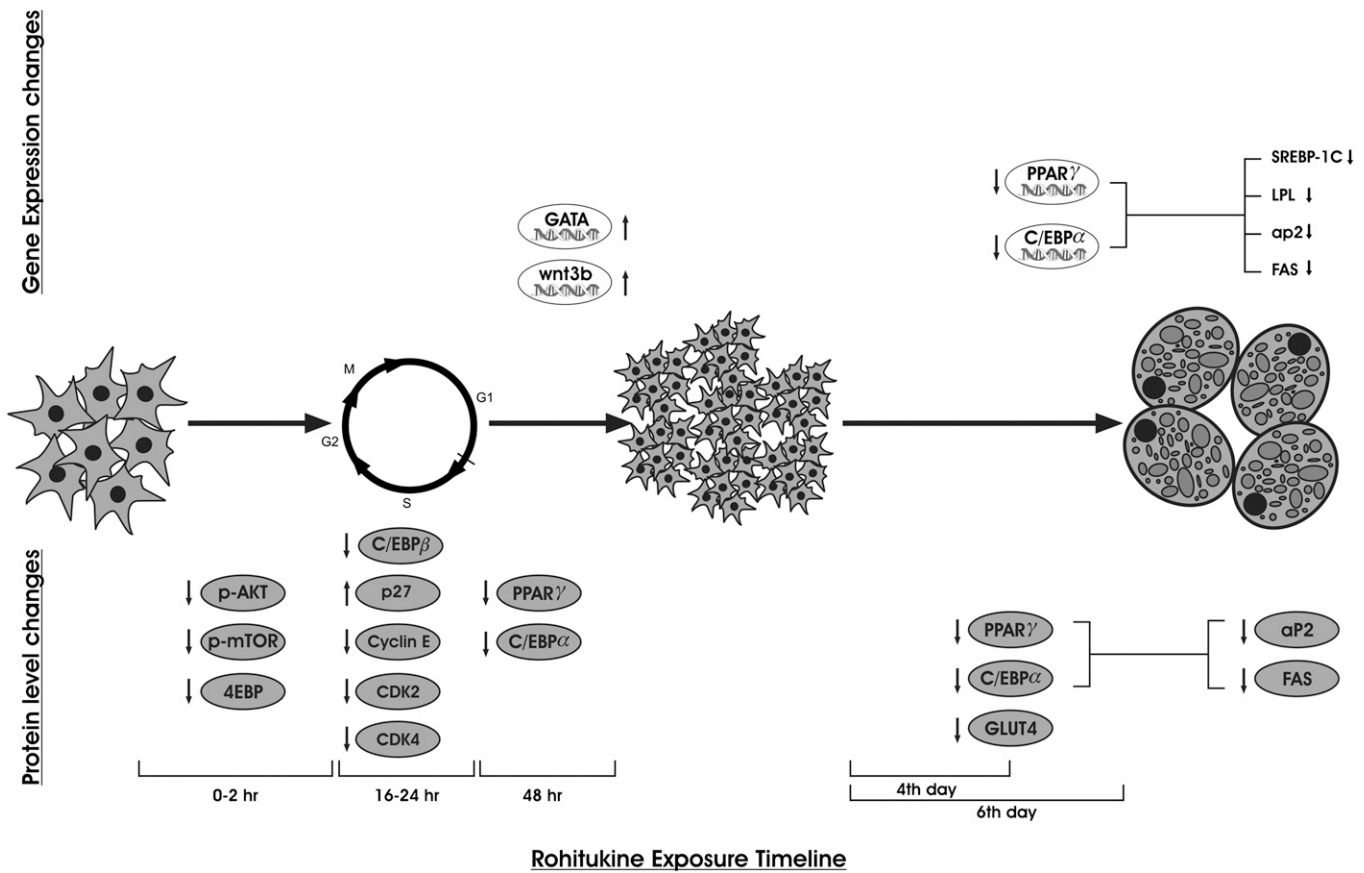



Fig. 6. Schematic presentation of time-dependent gene and protein level expression changes imparted by rohitukine addition to MDI during adipogenesis.

pterostilbene has also been reported to reduce the LDL/HDL-c ratio significantly in HFD-fed hypercholesterolemic hamsters (51). Mulberry water extract, which contains chlorogenic acid, rutin, gallic acid, and anthocyanins, was found to be hypolipidemic in a hamster model (52). A mixture of hesperidin and naringin has shown hypolipidemic activity in diet-induced hypercholesterolemic hamsters (49). The LA compound sinapinic acid had not been reported yet for anti-dyslipidemic or hypolipidemic activity. Besides this, well known anti-adipogenic compounds such as curcumin (46), cordycepin (39), berberine (53), piceatannol (43) and daidzein (54) also showed anti-dyslipidemic and hypolipidemic activity in a hamster model (51, 55–58). Most of the studies were conducted using the Syrian golden hamster because it is a very sensitive model system for changes in lipid profile when fed with HFD. Second, these hamsters have closer similarity to the human lipoprotein profile in comparisons with rats and mice (59). Thus, we decided to evaluate the effect of rohitukine in an HFD-fed hamster model. In view of the notable significant decrease in food consumption of the high dose-treated group by day 8 of the experiment, it was inevitable for us to perform studies with the PFD group (supplementary data and supplementary Fig. IV). We initially checked oral bioavailability, and rohitukine was readily bioavailable, with more than 25.7% absorbed within 30 min duration, and remained in circulation for more than 24 h. We then

modified the dose regimen to 50 mg/kg body weight. To evaluate the true contribution of rohitukine independent of diet consumption on changes in lipid parameters, we put one animal group on PFD. As shown in the results, there was a significant increase in TG, TC, LDL-c, and HDL-c in HFD as well as PFD groups when compared with normal chow. Rohitukine significantly decreased all of the previously mentioned parameters at the 50 mg/kg dose (Fig. 5B–D) and significantly increased the HDL-c/TC ratio (Fig. 5F). LXRα is the main regulator of lipid-controlling genes (60). It is also known that LXRα is a sensor of cholesterol excess (61), and its activation in dyslipidemic hamsters led to an increase in reverse cholesterol transport (62) and reduced lipid accumulation (63). SREBP-2 is involved in cholesterol synthesis (64), which in turn regulates expression of HMGCR and LDLR (65). All these gene expression levels in liver were found to be reduced in rohitukine-treated groups compared with the HFD-treated group (Fig. 5H), similar to that observed with fenofibrate, the standard anti-dyslipidemic agent (66). In adipocytes, 10 days of HFD intervention showed adipocyte hypertrophy as well as epididymal weight gain, which was reduced in the rohitukine-treated group. Rohitukine also reduced expression of PPARγ, FAS, αP2, and GLUT-4 proteins in gonadal fat tissue, indicating decreased fat turnover (Fig. 5G, I, J). Histological sections show that lipid accumulation was increased in hepatocytes in the HFD and PFD groups, while

rohitukine treatment decreased lipid accumulation and brought it back to near normal (Fig. 5K). Although it is beyond the scope of this manuscript to pinpoint the exact mechanism, similar to earlier demonstrated antiadipogenic molecules exhibiting antidyslipidemic activity, rohitukine also demonstrated in vivo antidyslipidemic effects.

Rohitukine derivatives, Flavopiridol and P-276-00, are currently being pursued in Phase II clinical trial for anticancer activity. The two compounds mapped well on Hypo-3 and CFPMA predicted fit values of 2.791 and 2.969, respectively, for these compounds. This may encourage researchers to explore novel antiadipogenic activities for these compounds. The pharmacophore mapping of these compounds has been presented in the supporting information (supplementary Fig. II).

In summary, our studies led to the development of the first pharmacophore model of antiadipogenic compounds for successful identification of rohitukine as the lead molecule. We showed that rohitukine possesses both antiadipogenic activity in vitro and antidyslipidemic activity in vivo. However, clinical development of rohitukine for these indications and chronic treatment is dependent on many other factors. Nevertheless, rohitukine is the parent pharmacophore of two leading molecules in the anticancer drug development pipeline, Flavopiridol and P-276-00, and both of them also map well for feature requirements of antiadipogenic compounds. It would be interesting to evaluate the antiadipogenic potential of these molecules and their impact on the outcome of clinical trials currently being conducted.

REFERENCES

- Ginsberg, H. N., and P. R. MacCallum. 2009. The obesity, metabolic syndrome, and type 2 diabetes mellitus pandemic: Part I. Increased cardiovascular disease risk and the importance of atherogenic dyslipidemia in persons with the metabolic syndrome and type 2 diabetes mellitus. *J. Cardiometab. Syndr.* **4**: 113–119.
- Adamczak, M., and A. Wiecek. 2013. The adipose tissue as an endocrine organ. *Semin. Nephrol.* **33**: 2–13.
- Taillan, B., J. G. Fuzibet, G. Garnier, A. Pesce, H. Vinti, M. C. Saint-Paul, and P. Dujardin. 1991. [Hepatic involvement in human immunodeficiency virus infection. 104 histologically documented cases]. *Ann. Med. Interne (Paris)*. **142**: 226–227. French.
- Zhang, M., K. Ikeda, J. W. Xu, Y. Yamori, X. M. Gao, and B. L. Zhang. 2009. Genistein suppresses adipogenesis of 3T3–L1 cells via multiple signal pathways. *Phytother. Res.* **23**: 713–718.
- Noto, A., P. Zahradka, N. Yurkova, X. Xie, H. Truong, E. Nitschmann, M. R. Ogborn, and C. G. Taylor. 2007. Dietary conjugated linoleic acid decreases adipocyte size and favorably modifies adipokine status and insulin sensitivity in obese, insulin-resistant rats. *Metabolism*. **56**: 1601–1611.
- Kim, H. K., M. Della-Fera, J. Lin, and C. A. Baile. 2006. Docosahexaenoic acid inhibits adipocyte differentiation and induces apoptosis in 3T3–L1 preadipocytes. *J. Nutr.* **136**: 2965–2969.
- Kim, H., and K. Sakamoto. 2012. (-)-Epigallocatechin gallate suppresses adipocyte differentiation through the MEK/ERK and PI3K/Akt pathways. *Cell Biol. Int.* **36**: 147–153.
- Yang, J. Y., M. A. Della-Fera, S. Rayalam, S. Ambati, D. L. Hartzell, H. J. Park, and C. A. Baile. 2008. Enhanced inhibition of adipogenesis and induction of apoptosis in 3T3–L1 adipocytes with combinations of resveratrol and quercetin. *Life Sci.* **82**: 1032–1039.
- Rayalam, S., J. Y. Yang, S. Ambati, M. A. Della-Fera, and C. A. Baile. 2008. Resveratrol induces apoptosis and inhibits adipogenesis in 3T3–L1 adipocytes. *Phytother. Res.* **22**: 1367–1371.
- Ambati, S., J. Y. Yang, S. Rayalam, H. J. Park, M. A. Della-Fera, and C. A. Baile. 2009. Ajoene exerts potent effects in 3T3–L1 adipocytes by inhibiting adipogenesis and inducing apoptosis. *Phytother. Res.* **23**: 513–518.
- Rayalam, S., M. A. Della-Fera, and C. A. Baile. 2008. Phytochemicals and regulation of the adipocyte life cycle. *J. Nutr. Biochem.* **19**: 717–726.
- Klebe, G., and U. Abraham. 1999. Comparative molecular similarity index analysis (CoMSIA) to study hydrogen-bonding properties and to score combinatorial libraries. *J. Comput. Aided Mol. Des.* **13**: 1–10.
- Klebe, G., U. Abraham, and T. Mietzner. 1994. Molecular similarity indices in a comparative analysis (CoMSIA) of drug molecules to correlate and predict their biological activity. *J. Med. Chem.* **37**: 4130–4146.
- Catalyst Version 4.1 ed. 2006. Accelrys Inc., San Diego, CA.
- Jain, S. K., S. B. Bharate, and R. A. Vishwakarma. 2012. Cyclin-dependent kinase inhibition by flavoalkaloids. *Mini Rev. Med. Chem.* **12**: 632–649.
- Singh, N., P. Singh, S. Shrivastva, S. K. Mishra, V. Lakshmi, R. Sharma, and G. Palit. 2012. Gastroprotective effect of anti-cancer compound rohitukine: possible role of gastrin antagonism and H(+) K(+) ATPase inhibition. *Naunyn Schmiedebergs Arch. Pharmacol.* **385**: 277–286.
- Mohana Kumara, P., S. Zuehlke, V. Priti, B. T. Ramesha, S. Shweta, G. Ravikanth, R. Vasudeva, T. R. Santhoshkumar, M. Spittler, and R. Uma Shaanker. 2012. Fusarium proliferatum, an endophytic fungus from *Dysoxylum binectariferum* Hook.f, produces rohitukine, a chromane alkaloid possessing anti-cancer activity. *Antonie van Leeuwenhoek*. **101**: 323–329.
- Keshri, G., R. M. Oberoi, V. Lakshmi, K. Pandey, and M. M. Singh. 2007. Contraceptive and hormonal properties of the stem bark of *Dysoxylum binectariferum* in rat and docking analysis of rohitukine, the alkaloid isolated from active chloroform soluble fraction. *Contraception*. **76**: 400–407.
- Lakshmi, V., K. Pandey, A. Kapil, N. Singh, M. Samant, and A. Dube. 2007. In vitro and in vivo leishmanicidal activity of *Dysoxylum binectariferum* and its fractions against *Leishmania donovani*. *Phytomedicine*. **14**: 36–42.
- Arguello, F., M. Alexander, J. A. Sterry, G. Tudor, E. M. Smith, N. T. Kalavar, J. F. Greene, Jr., W. Koss, C. D. Morgan, S. F. Stinson, et al. 1998. Flavopiridol induces apoptosis of normal lymphoid cells, causes immunosuppression, and has potent antitumor activity in vivo against human leukemia and lymphoma xenografts. *Blood*. **91**: 2482–2490.
- Du, G. J., Z. Zhang, X. D. Wen, C. Yu, T. Calway, C. S. Yuan, and C. Z. Wang. 2012. Epigallocatechin gallate (EGCG) is the most effective cancer chemopreventive polyphenol in green tea. *Nutrients*. **4**: 1679–1691.
- Hörmann, V., J. Kumi-Diaka, M. Durity, and A. Rathinavelu. 2012. Anticancer activities of genistein-topotecan combination in prostate cancer cells. *J. Cell. Mol. Med.* **16**: 2631–2636.
- Kang, J. W., J. H. Kim, K. Song, S. H. Kim, J. H. Yoon, and K. S. Kim. 2010. Kaempferol and quercetin, components of Ginkgo biloba extract (EGb 761), induce caspase-3-dependent apoptosis in oral cavity cancer cells. *Phytother. Res.* **24**: S77–S82.
- Vucenik, I., and J. P. Stains. 2012. Obesity and cancer risk: evidence, mechanisms, and recommendations. *Ann. N. Y. Acad. Sci.* **1271**: 37–43.
- Aballay, L. R., A. R. Eynard, P. Diaz Mdel, A. Navarro, and S. E. Munoz. 2013. Overweight and obesity: a review of their relationship to metabolic syndrome, cardiovascular disease, and cancer in South America. *Nutr. Rev.* **71**: 168–179.
- Ito, K., R. Ishigamori, M. Mutoh, T. Ohta, T. Imai, and M. Takahashi. 2013. The A allele promotes azoxymethane-induced colorectal carcinogenesis via macrophage migration in hyperlipidemic/diabetic KK mice. *Cancer Sci.* **104**: 835–843.
- Hsu, C. L., and G. C. Yen. 2007. Effects of flavonoids and phenolic acids on the inhibition of adipogenesis in 3T3–L1 adipocytes. *J. Agric. Food Chem.* **55**: 8404–8410.
- Brooks, R. B., R. E. Bruccoleri, B. D. Olafson, D. J. States, S. Swaminathan, and M. Karplus. 1983. CHARMM: a program for macromolecular energy, minimization, and dynamics calculations. *J. Comput. Chem.* **4**: 187–217.
- Smellie, A., S. L. Teig, and P. Towbin. 1995. Poling: promoting conformational variation. *J. Comput. Chem.* **16**: 171–187.
- Wu, Z., E. D. Rosen, R. Brun, S. Hauser, G. Adelmant, A. E. Troy, C. McKeon, G. J. Darlington, and B. M. Spiegelman. 1999.

- Cross-regulation of C/EBP alpha and PPAR gamma controls the transcriptional pathway of adipogenesis and insulin sensitivity. *Mol. Cell.* **3**: 151–158.
31. Rosen, E. D., C. H. Hsu, X. Wang, S. Sakai, M. W. Freeman, F. J. Gonzalez, and B. M. Spiegelman. 2002. C/EBPalpha induces adipogenesis through PPARgamma: a unified pathway. *Genes Dev.* **16**: 22–26.
 32. Hu, Y., and G. E. Davies. 2009. Berberine increases expression of GATA-2 and GATA-3 during inhibition of adipocyte differentiation. *Phytomedicine.* **16**: 864–873.
 33. Horikawa, T., T. Shimada, Y. Okabe, K. Kinoshita, K. Koyama, K. Miyamoto, K. Ichinose, K. Takahashi, and M. Aburada. 2012. Polymethoxyflavonoids from *Kaempferia parviflora* induce adipogenesis on 3T3–L1 preadipocytes by regulating transcription factors at an early stage of differentiation. *Biol. Pharm. Bull.* **35**: 686–692.
 34. Bennett, C. N., S. E. Ross, K. A. Longo, L. Bajnok, N. Hemati, K. W. Johnson, S. D. Harrison, and O. A. MacDougald. 2002. Regulation of Wnt signaling during adipogenesis. *J. Biol. Chem.* **277**: 30998–31004.
 35. Avruch, J. 1998. Insulin signal transduction through protein kinase cascades. *Mol. Cell. Biochem.* **182**: 31–48.
 36. Morgan, T. M., T. D. Koreckij, and E. Corey. 2009. Targeted therapy for advanced prostate cancer: inhibition of the PI3K/Akt/mTOR pathway. *Curr. Cancer Drug Targets.* **9**: 237–249.
 37. Wu, K., C. Wang, M. D'Amico, R. J. Lee, C. Albanese, R. G. Pestell, and S. Mani. 2002. Flavopiridol and trastuzumab synergistically inhibit proliferation of breast cancer cells: association with selective cooperative inhibition of cyclin D1-dependent kinase and Akt signaling pathways. *Mol. Cancer Ther.* **1**: 695–706.
 38. Zhang, H. H., J. Huang, K. Duvel, B. Boback, S. Wu, R. M. Squillace, C. L. Wu, and B. D. Manning. 2009. Insulin stimulates adipogenesis through the Akt-TSC2-mTORC1 pathway. *PLoS ONE.* **4**: e6189.
 39. Takahashi, S., M. Tamai, S. Nakajima, H. Kato, H. Johno, T. Nakamura, and M. Kitamura. 2012. Blockade of adipocyte differentiation by cordycepin. *Br. J. Pharmacol.* **167**: 561–575.
 40. Wei, Z., M. M. Seldin, N. Natarajan, D. C. Djemal, J. M. Peterson, and G. W. Wong. 2013. C1q/TNF-related protein 11 (CTRP11), a novel adipose stroma-derived regulator of adipogenesis. *J. Biol. Chem.* **288**: 10214–10229.
 41. Choi, K. M., Y. S. Lee, D. M. Sin, S. Lee, M. K. Lee, Y. M. Lee, J. T. Hong, Y. P. Yun, and H. S. Yoo. 2012. Sulforaphane inhibits mitotic clonal expansion during adipogenesis through cell cycle arrest. *Obesity (Silver Spring).* **20**: 1365–1371.
 42. Kwon, J. Y., S. G. Seo, S. Yue, J. X. Cheng, K. W. Lee, and K. H. Kim. 2012. An inhibitory effect of resveratrol in the mitotic clonal expansion and insulin signaling pathway in the early phase of adipogenesis. *Nutr. Res.* **32**: 607–616.
 43. Kwon, J. Y., S. G. Seo, S. H. Heo, S. Yue, J. X. Cheng, K. W. Lee, and K. H. Kim. 2012. Piceatannol, natural polyphenolic stilbene, inhibits adipogenesis via modulation of mitotic clonal expansion and insulin receptor-dependent insulin signaling in early phase of differentiation. *J. Biol. Chem.* **287**: 11566–11578.
 44. Tidhar, Y., H. Weissman, S. G. Wolf, A. Gulino, and B. Rybtchinski. 2011. Pathway-dependent self-assembly of perylene diimide/peptide conjugates in aqueous medium. *Chemistry.* **17**: 6068–6075.
 45. Yun, H. J., J. H. Kim, H. Y. Jeong, H. H. Ji, S. W. Nam, E. W. Lee, B. W. Kim, and H. J. Kwon. 2012. Widdrol blocks 3T3–L1 preadipocytes growth and differentiation due to inhibition of mitotic clonal expansion. *J. Microbiol. Biotechnol.* **22**: 806–813.
 46. Kim, C. Y., T. T. Le, C. Chen, J. X. Cheng, and K. H. Kim. 2011. Curcumin inhibits adipocyte differentiation through modulation of mitotic clonal expansion. *J. Nutr. Biochem.* **22**: 910–920.
 47. Hsu, C. L., Y. J. Lin, C. T. Ho, and G. C. Yen. 2012. Inhibitory effects of garcinol and pterostilbene on cell proliferation and adipogenesis in 3T3–L1 cells. *Food Funct.* **3**: 49–57.
 48. Kalgankar, S., H. B. Gross, W. Yokoyama, and C. L. Keen. 2010. Effects of a flavonol-rich diet on select cardiovascular parameters in a Golden Syrian hamster model. *J. Med. Food.* **13**: 108–115.
 49. Kurowska, E. M., and J. A. Manthey. 2004. Hypolipidemic effects and absorption of citrus polymethoxylated flavones in hamsters with diet-induced hypercholesterolemia. *J. Agric. Food Chem.* **52**: 2879–2886.
 50. Auger, C., P. L. Teissedre, P. Gerain, N. Lequeux, A. Bornet, S. Serisier, P. Besancon, B. Caporiccio, J. P. Cristol, and J. M. Rouanet. 2005. Dietary wine phenolics catechin, quercetin, and resveratrol efficiently protect hypercholesterolemic hamsters against aortic fatty streak accumulation. *J. Agric. Food Chem.* **53**: 2015–2021.
 51. Rimando, A. M., R. Nagmani, D. R. Feller, and W. Yokoyama. 2005. Pterostilbene, a new agonist for the peroxisome proliferator-activated receptor alpha-isoform, lowers plasma lipoproteins and cholesterol in hypercholesterolemic hamsters. *J. Agric. Food Chem.* **53**: 3403–3407.
 52. Peng, C. H., L. K. Liu, C. M. Chuang, C. C. Chyau, C. N. Huang, and C. J. Wang. 2011. Mulberry water extracts possess an anti-obesity effect and ability to inhibit hepatic lipogenesis and promote lipolysis. *J. Agric. Food Chem.* **59**: 2663–2671.
 53. Huang, C., Y. Zhang, Z. Gong, X. Sheng, Z. Li, W. Zhang, and Y. Qin. 2006. Berberine inhibits 3T3–L1 adipocyte differentiation through the PPARgamma pathway. *Biochem. Biophys. Res. Commun.* **348**: 571–578.
 54. Kim, M. H., J. S. Park, M. S. Seo, J. W. Jung, Y. S. Lee, and K. S. Kang. 2010. Genistein and daidzein repress adipogenic differentiation of human adipose tissue-derived mesenchymal stem cells via Wnt/beta-catenin signalling or lipolysis. *Cell Prolif.* **43**: 594–605.
 55. Jang, E. M., M. S. Choi, U. J. Jung, M. J. Kim, H. J. Kim, S. M. Jeon, S. K. Shin, C. N. Seong, and M. K. Lee. 2008. Beneficial effects of curcumin on hyperlipidemia and insulin resistance in high-fat-fed hamsters. *Metabolism.* **57**: 1576–1583.
 56. Guo, P., Q. Kai, J. Gao, Z. Q. Lian, C. M. Wu, C. A. Wu, and H. B. Zhu. 2010. Cordycepin prevents hyperlipidemia in hamsters fed a high-fat diet via activation of AMP-activated protein kinase. *J. Pharmacol. Sci.* **113**: 395–403.
 57. Kong, W., J. Wei, P. Abidi, M. Lin, S. Inaba, C. Li, Y. Wang, Z. Wang, S. Si, H. Pan, et al. 2004. Berberine is a novel cholesterol-lowering drug working through a unique mechanism distinct from statins. *Nat. Med.* **10**: 1344–1351.
 58. Song, T., S. O. Lee, P. A. Murphy, and S. Hendrich. 2003. Soy protein with or without isoflavones, soy germ and soy germ extract, and daidzein lessen plasma cholesterol levels in golden Syrian hamsters. *Exp. Biol. Med. (Maywood).* **228**: 1063–1068.
 59. Zhang, Z., H. Wang, R. Jiao, C. Peng, Y. M. Wong, V. S. Yeung, Y. Huang, and Z. Y. Chen. 2009. Choosing hamsters but not rats as a model for studying plasma cholesterol-lowering activity of functional foods. *Mol. Nutr. Food Res.* **53**: 921–930.
 60. Nuclear Receptor Nomenclature Committee. 1999. A unified nomenclature system for the nuclear receptor superfamily. *Cell.* **97**: 161–163.
 61. Chawla, A., J. J. Repa, R. M. Evans, and D. J. Mangelsdorf. 2001. Nuclear receptors and lipid physiology: opening the X-files. *Science.* **294**: 1866–1870.
 62. Briand, F., M. Treguier, A. Andre, D. Grillot, M. Issandou, K. Ouguerram, and T. Sulpice. 2010. Liver X receptor activation promotes macrophage-to-feces reverse cholesterol transport in a dyslipidemic hamster model. *J. Lipid Res.* **51**: 763–770.
 63. Mukherjee, R., K. T. Locke, B. Miao, D. Meyers, H. Monshizadegan, R. Zhang, D. Search, D. Grimm, M. Flynn, K. M. O'Malley, et al. 2008. Novel peroxisome proliferator-activated receptor alpha agonists lower low-density lipoprotein and triglycerides, raise high-density lipoprotein, and synergistically increase cholesterol excretion with a liver X receptor agonist. *J. Pharmacol. Exp. Ther.* **327**: 716–726.
 64. König, B., A. Koch, J. Spielmann, C. Hilgenfeld, G. I. Stangl, and K. Eder. 2007. Activation of PPARalpha lowers synthesis and concentration of cholesterol by reduction of nuclear SREBP-2. *Biochem. Pharmacol.* **73**: 574–585.
 65. Van Rooyen, D. M., and G. C. Farrell. 2011. SREBP-2: a link between insulin resistance, hepatic cholesterol, and inflammation in NASH. *J. Gastroenterol. Hepatol.* **26**: 789–792.
 66. Guo, Q., P. R. Wang, D. P. Milot, M. C. Ippolito, M. Hernandez, C. A. Burton, S. D. Wright, and Y. Chao. 2001. Regulation of lipid metabolism and gene expression by fenofibrate in hamsters. *Biochim. Biophys. Acta.* **1533**: 220–232.